

Accepted Manuscript

Identification of Amides Derived From 1*H*-Pyrazolo[3,4-*b*]pyridine-5-carboxylic Acid as Potent Inhibitors of Human Nicotinamide Phosphoribosyltransferase (NAMPT)

Xiaozhang Zheng, Kenneth W. Bair, Paul Bauer, Timm Baumeister, Krista K. Bowman, Alexandre J. Buckmelter, Maureen Caligiuri, Karl H. Clodfelter, Yezhen Feng, Bingsong Han, Yen-Ching Ho, Nikolai Kley, Hong Li, Xiaorong Liang, Bianca M. Liederer, Jian Lin, Justin Ly, Thomas O'Brien, Jason Oeh, Angela Oh, Dominic J. Reynolds, Deepak Sampath, Geeta Sharma, Nicholas Skelton, Chase C. Smith, Jarrod Tremayne, Leslie Wang, Weiru Wang, Zhongguo Wang, Hongxing Wu, Jiansheng Wu, Yang Xiao, Guangxing Yang, Po-wai Yuen, Mark Zak, Peter S. Dragovich

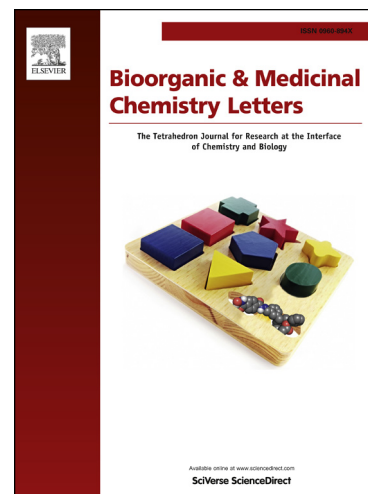
PII: S0960-894X(13)01014-7
DOI: <http://dx.doi.org/10.1016/j.bmcl.2013.08.074>
Reference: BMCL 20812

To appear in: *Bioorganic & Medicinal Chemistry Letters*

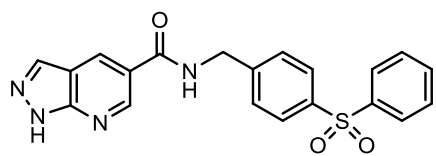
Received Date: 14 July 2013
Revised Date: 11 August 2013
Accepted Date: 15 August 2013

Please cite this article as: Zheng, X., Bair, K.W., Bauer, P., Baumeister, T., Bowman, K.K., Buckmelter, A.J., Caligiuri, M., Clodfelter, K.H., Feng, Y., Han, B., Ho, Y-C., Kley, N., Li, H., Liang, X., Liederer, B.M., Lin, J., Ly, J., O'Brien, T., Oeh, J., Oh, A., Reynolds, D.J., Sampath, D., Sharma, G., Skelton, N., Smith, C.C., Tremayne, J., Wang, L., Wang, W., Wang, Z., Wu, H., Wu, J., Xiao, Y., Yang, G., Yuen, P-w., Zak, M., Dragovich, P.S., Identification of Amides Derived From 1*H*-Pyrazolo[3,4-*b*]pyridine-5-carboxylic Acid as Potent Inhibitors of Human Nicotinamide Phosphoribosyltransferase (NAMPT), *Bioorganic & Medicinal Chemistry Letters* (2013), doi: <http://dx.doi.org/10.1016/j.bmcl.2013.08.074>

This is a PDF file of an unedited manuscript that has been accepted for publication. As a service to our customers we are providing this early version of the manuscript. The manuscript will undergo copyediting, typesetting, and review of the resulting proof before it is published in its final form. Please note that during the production process errors may be discovered which could affect the content, and all legal disclaimers that apply to the journal pertain.

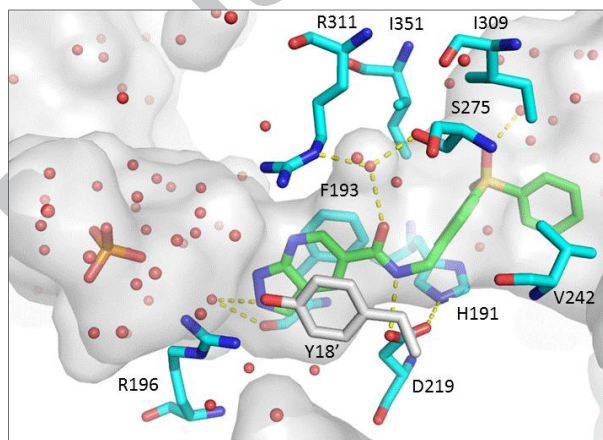


Graphical Abstract.



NAMPT BC IC₅₀ = 54 nM

A2780 Cell IC₅₀ = 66 nM



Identification of Amides Derived From 1*H*-Pyrazolo[3,4-*b*]pyridine-5-carboxylic Acid as Potent Inhibitors of Human Nicotinamide Phosphoribosyltransferase (NAMPT)

Xiaozhang Zheng^b, Kenneth W. Bair^b, Paul Bauer^b, Timm Baumeister^b, Krista K. Bowman^a, Alexandre J. Buckmelter^b, Maureen Caligiuri^b, Karl H. Clodfelter^b, Yezhen Feng^c, Bingsong Han^b, Yen-Ching Ho^b, Nikolai Kley^b, Hong Li^a, Xiaorong Liang^a, Bianca M. Liederer^a, Jian Lin^b, Justin Ly^a, Thomas O'Brien^a, Jason Oeh^a, Angela Oh^a, Dominic J. Reynolds^b, Deepak Sampath^a, Geeta Sharma^b, Nicholas Skelton^a, Chase C. Smith^b, Jarrod Tremayne^a, Leslie Wang^a, Weiru Wang^a, Zhongguo Wang^b, Hongxing Wu^c, Jiansheng Wu^a, Yang Xiao^a, Guangxing Yang^c, Po-wai Yuen^c, Mark Zak^a, Peter S. Dragovich^{a,*}

^aGenentech, Inc., 1 DNA Way, South San Francisco, California 94080, USA

^bForma Therapeutics, Inc., 500 Arsenal Street, Watertown, Massachusetts 02472, USA.

^cPharmaron Beijing, Co. Ltd., 6 Taihe Road, BDA, Beijing, 100176, P.R. China.

Abstract. Potent, 1*H*-pyrazolo[3,4-*b*]pyridine-containing inhibitors of the human nicotinamide phosphoribosyltransferase (NAMPT) enzyme were identified using structure-based design techniques. Many of these compounds exhibited nanomolar antiproliferation activities against human tumor lines in *in vitro* cell culture experiments, and a representative example (compound **26**) demonstrated encouraging *in vivo* efficacy in a mouse xenograft tumor model derived from the A2780 cell line. This molecule also exhibited reduced rat retinal exposures relative to a previously studied imidazo-pyridine-containing NAMPT inhibitor. Somewhat surprisingly, compound **26** was only weakly active *in vitro* against mouse and monkey tumor cell lines even though it was a potent inhibitor of NAMPT enzymes derived from these species. The compound also exhibited only minimal effects on *in vivo* NAD levels in mice, and these changes were considerably less profound than those produced by an imidazo-pyridine-containing NAMPT

inhibitor. The crystal structures of compound **26** and the corresponding PRPP-derived ribose adduct in complex with NAMPT were also obtained.

Keywords: nicotinamide phosphoribosyltransferase, NAMPT, X-ray crystal structure, tumor metabolism.

ACCEPTED MANUSCRIPT

The conversion of nicotinamide (NAM) to the biologically important enzyme co-factor nicotinamide adenine dinucleotide (NAD) is accomplished in mammalian cells by the two-step process depicted in Figure 1.¹ Nicotinamide phosphoribosyltransferase (NAMPT; also known in the literature as pre-B cell colony-enhancing factor/PBEF and visfatin) catalyzes the first and rate-limiting step in this transformation in which nicotinamide (NAM) is condensed with phosphoribosyl pyrophosphate (PRPP) to produce nicotinamide mononucleotide (NMN; Figure 1).² Although covalent modification of NAM and/or PRPP by NAMPT is not believed to occur during this conversion, efficient production of NMN is dependent on the phosphorylation of a histidine residue in the NAMPT active site by ATP.² NAM is produced by the normal function of NAD-consuming enzymes such as PARPs and sirtuins, and the described NAM-NAD conversion represents the only known mechanism for mammalian cells to efficiently recycle NAM back to NAD.³ Accordingly, blocking NAMPT activity may impair the maintenance of intracellular NAD levels, and this disruption may negatively impact the growth and/or function of cells which are highly reliant on NAD-dependent processes for survival. As many tumors and/or cancer cell lines exhibit elevated metabolisms and high proliferation rates, NAMPT inhibition is currently viewed as a novel strategy for the development of new anticancer agents.⁴

Multiple examples of NAMPT inhibitors have been previously described in the scientific and patent literature.^{2a,2b} The most advanced of these agents, GMX-1778⁵ (**1**), its prodrug GMX-1777⁶ (not shown), and APO-866⁷ (**2**) progressed to clinical trials during the past decade (Figure 2). In addition, our own NAMPT inhibitor discovery efforts recently identified amide-containing sulfonamides and sulfones exemplified by compounds **3** and **4** (Figure 2).^{8,9} One concern associated with the development of NAMPT inhibitors is that they may exhibit undesired toxicities toward normal (non-cancerous) tissues, particularly those which are metabolically

active. Indeed, retinal atrophy was reported in pre-clinical rodent safety assessments with APO-866, although such effects were not observed in related monkey studies.^{7b} In addition, mutations in NMNAT, the enzyme which catalyzes the second step in the NAM-NAD conversion (c.f., Figure 1), were recently shown to cause serious retinal defects in humans (Leber congenital amaurosis; LCA).¹⁰ While it is currently uncertain whether the mutant NMNAT outcomes are related to the protein's ability to produce NAD,¹¹ the collective data described above suggest that inhibiting the NAM-NAD conversion has the possibility to detrimentally impact the health of retinal tissue.¹²

We therefore sought to identify NAMPT inhibitors which exhibited reduced retinal penetration and/or retention relative to the molecules we had previously studied. If mechanism-based retinal toxicities were to be encountered with the previously-studied compounds, the new entities might be able to attenuate these unwanted effects.¹³ Accordingly, we implemented a physiochemical-based design strategy to minimize the blood-retina barrier penetration and/or the retinal retention times of newly-synthesized NAMPT inhibitors.¹⁴ In particular, we sought to identify compounds devoid of basic centers (even weakly basic ones) as protonation of such sites was believed to contribute greatly to long retinal retention.¹⁴ This aspect of the new inhibitor design posed a significant challenge since all potent, cell-active NAMPT inhibitors described to date contain a weakly basic heterocyclic nitrogen atom believed to participate in an enzyme-catalyzed condensation with PRPP in the protein's active site (e.g., imidazo-pyridine-containing inhibitors such as **5** are converted to PRPP-adducts **7**; Figure 3).¹⁵ We hypothesized that isosteric (and less-basic) indazole-derived inhibitors might form similar PRPP adducts in the NAMPT active site and thereby also function as potent cell-active inhibitors of the enzyme (e.g., conversion of **6** to **8**; Figure 3). In this report, we describe the successful identification of

indazole-derived NAMPT inhibitors along with their detailed biological and structural characterization.

As shown in Table 1, incorporation of a simple indazole into the inhibitor design afforded a compound that was a significantly weaker NAMPT inhibitor than the corresponding imidazopyridine-containing molecule (compare **10** with **3**). Introduction of nitrogen atoms at the 4 and 6-positions on the 5-carboxy-indazole ring system also afforded weakly active NAMPT inhibitors (compare **11** and **12** with **9**, Table 1). However, a molecule containing an amide derived from 1*H*-pyrazolo[3,4-*b*]pyridine-5-carboxylic acid (**13**; i.e., incorporation of a nitrogen at the 7-position of the 5-carboxy-indazole ring system) displayed relatively potent biochemical NAMPT inhibition and was also active in an A2780 cell-based assessment.^{16,17} Similar inhibition activities were observed when a phenyl sulfone moiety was incorporated at the inhibitor terminus in lieu of the piperidine-derived sulfonamide (**14**). However, methylation of the indazole NH group present in **14** or removal of the other indazole nitrogen atom was highly detrimental to anti-NAMPT activity (compare compounds **15** and **16** with **14**).

To facilitate further optimization of the 1*H*-pyrazolo[3,4-*b*]pyridine-containing compounds, an X-ray crystal structure of compound **14** in complex with the NAMPT protein was determined.¹⁸ As shown in Figure 4, the compound bound in a cleft formed between two monomers of the NAMPT protein and extended from this binding site out towards solvent. The 1*H*-pyrazolo[3,4-*b*]pyridine ring system formed a face-to-face pi-stack with Phe193 of one NAMPT monomer and with Tyr18' of the other in a manner that likely mimics nicotinamide binding to the same region. The N-2 nitrogen atom in the 1*H*-pyrazolo[3,4-*b*]pyridine ring was hydrogen bonded to a water molecule in the active site, which also formed a hydrogen bond to the backbone carbonyl oxygen of Phe293. A phosphate ion, likely originating from the

crystallization buffer, was also observed in the active site cleft, and this entity was coordinated by the side chains of Arg392', Ser398' and Lys400' (for clarity, these side chains are not depicted in Figure 4). In addition, nine water molecules were noted within hydrogen-bonding distance of the phosphate oxygen atoms. The amide portion of **14** occupied a more polar NAMPT pocket and formed hydrogen bonds with the side chain of Asp219 and a neighboring water molecule (which itself was hydrogen bonded to the side chains of Arg311 and Ser275). The bisphenyl sulfone moiety present in **14** made non-bonded contacts with the side chains of Ile351, Ile309 and Val242 in a much more hydrophobic portion of the binding site. The phenyl group proximal to the amide also formed an edge-to-face pi-stack with His191, whereas the distal phenyl moiety projected into the solvent exposed entrance of the binding cleft. A hydrogen bond between one of the **14** sulfone oxygen atoms and a solvent water molecule was also observed.

With the above structural information in hand, we next sought to further improve the biochemical and cell-based inhibition properties of the new inhibitor series. As shown in Table 2, incorporation of sulfonamides derived from substituted piperidines or piperazines (**17-22**), morpholine (**23**), or a spirocyclic azetidine (**24**) into the inhibitor design was generally tolerated. However, none of these entities was significantly more active than the lead compound containing an unsubstituted piperidine-derived sulfonamide (**13**). In contrast, inhibitors incorporating various substituted phenyl sulfones displayed dramatically improved anti-NAMPT properties in both biochemical and cell-based assessments relative to the unsubstituted analog (compare **25-27** with **14**, Table 2). Similar, incorporation of terminal sulfones containing various heteroaromatic groups also typically afforded very potent biochemical and cell-based NAMPT inhibitors (**28-35**, Table 2; exception = **33**). Encouragingly, the majority of the compounds depicted in Table 2,

especially the diaryl-sulfones, exhibited acceptable stability (stable to moderate) toward human liver microsomes when tested in an *in vitro* assay.

In preparation for conducting *in vivo* experiments with the new class of NAMPT inhibitors, we profiled several of the most potent examples in a variety of additional *in vitro* DMPK assessments. As shown in Table 3, all compounds examined were relatively labile toward mouse liver microsomes, but all exhibited improved metabolic stability properties when the assessment was performed using mouse hepatocytes. The molecules displayed a range of permeabilities as determined in an MDCK cell monolayer assay with the more polar entities unsurprisingly exhibiting the lower values. The compounds were typically highly bound to mouse plasma proteins but one example (**25**) exhibited higher free fraction than the others. The solubility of the molecules depicted in Table 3 was generally very poor with the values for many compounds residing below the limit of the high throughput assessment used to measure this property. However, compound **26** was an exception to this trend, and it exhibited measurable (albeit low) solubility in the high throughput assay. Importantly, the other Table 3 data associated with **26** collectively indicated that it possessed an ideal combination of potent NAMPT inhibition activity and attractive *in vitro* DMPK properties. Based on these favorable characteristics, compound **26** was therefore progressed to *in vivo* mouse PK and xenograft efficacy studies.

As shown in Figure 5 and Table 4, inhibitor **26** exhibited encouraging plasma exposures and PK parameters following IV and oral administration to female NCR nude mice. Single-dose IV administration of the compound determined that the molecule's *in vivo* mouse CL value was lower than that predicted from the *in vitro* mouse microsome and hepatocyte stability assessments (c.f., Table 3). This difference is potentially due to the high plasma protein binding

exhibited by the molecule. Importantly, QD administration of **26** at 100 mg/kg afforded free mouse plasma levels which exceeded the compound's A2780 antiproliferation cell culture IC₅₀ values for approximately 24 h (Figure 5). Accordingly, compound **26** displayed robust efficacy in an A2780 ovarian cancer xenograft model with relatively minor decreases in body weights when dosed orally at 100 mg/kg for 5 consecutive days (Figure 6A; see supplementary data for additional details). Notably, durable tumor regressions were observed in this experiment that were maintained even after compound dosing was discontinued. In addition, tumor NAD levels measured 1 hour after the day-5 dose of compound **26** were significantly reduced relative to the levels observed in tumors from vehicle treated animals (Figure 6B). Similar reductions in tumor NAD levels were also noted 24 hours after the day-5 compound **26** dose (Figure 6B). Encouragingly, and consistent with the design strategy outlined in the beginning of this work, compound **26** exhibited reduced retinal exposures relative to the imidazo-pyridine-containing inhibitor **4** when this property was assessed at both 1 and 6.5 hours following separate oral administration of the compounds to rats (Table 5; the differences were more apparent when the retina levels were normalized with respect to the corresponding plasma concentrations).¹⁹ As described above, these reduced exposures likely result from the attenuated basicity of compound **26** relative to **4** (measured pKa's = <2.0 and 5.3, respectively), but other factors such as logD (**26** = 3.4; **4** = 3.2) and/or TPSA (**26** = 104; **4** = 80) differences may also be responsible.¹⁴

In anticipation of conducting animal toxicology experiments with compound **26**, the molecule was biochemically profiled against NAMPT enzymes derived from animal species commonly used in such assessments. The imidazo-pyridine-containing inhibitor **4** was similarly examined, since its use in related toxicology studies was also being considered. As shown in Table 6, the biochemical IC₅₀ inhibition values for each compound varied <12-fold across the

different enzymes tested, with the most potent inhibition consistently observed against human NAMPT. A <3.5-fold variation in IC₅₀ values was also noted when the two compounds were tested against the same NAMPT isoform. However, since our prior experience indicated that potent biochemical NAMPT inhibitors did not always function as potent cell-active molecules,^{6,8,15} we also examined compounds **4** and **26** in a variety of *in vitro* assessments employing cell-lines from the same animal species. As shown in Table 7, compound **4** displayed potent or moderate anti-NAMPT cell activity in all lines against which it was tested. In stark contrast, however, compound **26** displayed negligible activity in mouse and monkey-derived cell lines and only exhibited potent antiproliferation effects in human and dog cells. This unexpected finding prompted us to conduct several additional experiments to verify and better understand the species activity differences associated with compound **26**.

As shown in Table 8, compound **26** failed to significantly reduce NAD levels in mouse KPP cells unless relatively high concentrations were employed while large mouse cell NAD reductions were induced by comparably low levels of compound **4** (see also Figure S1 in the supplementary data). In contrast, both compounds potently inhibited NAD levels in the human-derived PC3 cell line (Table 8, Figure S1). Importantly, intracellular quantitation of each compound in the murine KPP and human PC3 lines showed similar concentrations of **4** and **26** with no obvious difference in the levels of **26** present in the KPP (insensitive) and PC3 (sensitive) cells (Table 8). The ability of each compound to form NAMPT-catalyzed PRPP adducts in biochemical experiments was also assessed,¹⁵ and no distinction among them was observed (each compound formed the corresponding PRPP adduct with NAMPT enzyme from all five species; see supplementary data). Thus, examination of two obvious explanations for the described cell-based discrepancies failed to improve our understanding of the phenomenon.

To confirm that the cell-culture results depicted in Table 7 translated into *in vivo* outcomes, we performed a 5-day PK-PD study with compounds **4** and **26** in nude mice. In order to maximize the observed *in vivo* effects, we employed the highest tolerable doses of each molecule in this experiment (**4** = 30 mg/kg QD; **26** = 100 mg/kg QD). This dosing regimen afforded much higher mouse exposures of inhibitor **26** relative to compound **4** (supplementary data, Figure S5A).²⁰ In spite of these exposure differences, administration of inhibitor **4** resulted in more pronounced reductions in day-5 mouse blood NAD levels relative to those observed for compound **26** (Figure S5B). Differing effects on NAD levels were also noted in eye tissue sampled from animals in both dosing groups with compound **26** having minimal impact (Figure S5C). The attenuated effect of **26** in eye tissue relative to its activity in blood is consistent with the low retina/plasma ratio observed for the molecule in rat PK experiments (c.f., Table 5). Collectively, the PK-PD data show that high exposures of compound **26** afforded less pronounced effects on NAD levels in mice relative to those produced by much lower exposures of inhibitor **4**. Thus, the *in vivo* mouse PK-PD results are consistent with the Table 7 cell culture data which indicate that compound **26** exhibits dramatically attenuated potency in mouse cell lines relative to compound **4**.²¹

We also obtained a crystal structure of the PRPP-ribosylated adduct corresponding to compound **26** in complex with human NAMPT to determine whether analysis of its binding to the protein might help explain the above biological outcomes.²² As shown in Figure 7, the non-ribose atoms of the adduct were observed in locations very similar to those occupied by the corresponding atoms of inhibitor **14** (c.f., Figure 4; RMSD = 0.29 Å for 28 common ligand heavy atoms after superposition of the dimer protein chains). The backbone fold of NAMPT was also very similar in complex with compound **14** and compound **26** (RMSD 0.15 Å for 444 C-

alpha atoms in a single NAMPT protomer, as defined by the protein alignment tool in PyMOL), and the side chains lining the inhibitor binding cleft were located in very similar positions in both structures (compare Figures 4 and 7). Thus, the protein-ligand interactions involving non-ribose portions of the ligands were identical in the two structures. A similar binding orientation was also observed for compound **4** and its corresponding ribose adduct.^{8,23} In contrast to the complex with inhibitor **14**, there was no electron density observed for water molecules adjacent to the N-2 indazole nitrogen or the amide carbonyl oxygen of the **26**-ribose adduct. This difference may be due to the different resolutions of the two structures (1.75 vs 2.40 Å). Importantly, the 1.5 Å separation between the N-1 indazole nitrogen of **26** and the 1' ribose carbon atom clearly indicated the formation of a covalent bond between the two entities. The phospho-ribose portion of the **26**-ribose adduct formed several hydrogen bonds with the NAMPT protein involving the Arg311 side chain (to the ribose 2' hydroxyl), the Asp313 side chain (also to the ribose 2' hydroxyl), and the backbone amide NH of Gly384 (to an oxygen of the 5' phosphate group). There were also five water molecules observed within hydrogen bonding distance of the adduct (one to the 2' hydroxyl, one bridging between the 2' and 3' hydroxyl groups, and three proximal to the 5'-phosphate oxygen atoms).

Interestingly, the ligand binding site in the above crystal structure contained a well-resolved pyrophosphate group held in place by hydrogen bond interactions with the side chains of NAMPT residues Arg40', Arg392', Ser398', Lys400' and Lys423' (Figure 7; side chains not shown for clarity). One of the terminal oxygen atoms of this pyrophosphate group was located 3.5 Å from the C1' ribose atom of the **26**-ribose adduct (red dotted line in Figure 7). Given the nearly linear relationship between the pyrophosphate oxygen, ribose carbon, and inhibitor 1*H*-pyrazolo[3,4-*b*]pyridine nitrogen atoms (155 °), it is possible that Figure 7 depicts the conclusion

of a NAMPT-catalyzed process in which pyrophosphate is displaced from PRPP by the 1*H*-pyrazolo[3,4-*b*]pyridine N-1 nitrogen atom (c.f., Figure 3). The dense network of H-bond interactions formed between NAMPT and the pyrophosphate moiety suggest that the enzyme preorders the PRPP co-factor and a suitable substrate (an inhibitor such as **26** or the natural ligand NAM) and thereby facilitates the nucleophilic displacement of pyrophosphate from PRPP. Recent kinetic isotope measurements and quantum calculations performed on the PRPP-NAM transition state geometry also support this possibility.²⁴

In this work, we describe the identification of potent NAMPT inhibitors which contain the bicyclic 1*H*-pyrazolo[3,4-*b*]pyridine ring system. Many of these compounds exhibit nanomolar antiproliferation activity against human tumor lines in *in vitro* cell culture experiments, and a representative example (compound **26**) demonstrated encouraging *in vivo* efficacy in an A2780 mouse xenograft tumor model. However, compound **26** was also shown to lack meaningful *in vitro* activity against mouse and monkey cell lines even though it inhibited the NAMPT enzymes derived from these species. Such cell culture differences were not observed for a previously described NAMPT inhibitor which contains an imidazo-pyridine in lieu of the 1*H*-pyrazolo[3,4-*b*]pyridine ring system (compound **4**). Importantly, the mouse cell potencies observed for **4** and **26** correlated well with the ability of each compound to alter *in vivo* NAD levels in both blood and eye tissue. The observed cell potency differences may thus impact other *in vivo* outcomes in the associated animal species (e.g., safety assessments), and it is therefore suggested that appropriate cell culture profiling of promising NAMPT inhibitors be completed prior to conducting detailed *in vivo* studies with them.

Acknowledgements

We thank the members of the Genentech protein expression group for their help in expressing the NAMPT proteins used in this work. We also thank the DMPK group at Genentech, especially Jonathan Cheong, and Ning Liu, for their contribution to the generation of the DMPK data, Rashida Garcia-Dancey and Shohini Ganguly for helping to generate the cellular data, and Agilent Technologies (Woburn, MA) for generating the Rapidfire LCMS data. In addition, we acknowledge the use of the synchrotron X-ray source at ALS supported by the Department of Energy's (DOE) Office of Science. We also appreciate many helpful discussions regarding NAMPT with Drs. Peter Jackson and Marcia Belvin.

Supplementary data

Supplementary data associated with this article can be found in the online version at <http://XXXXXX>

References and notes

- (a) Houtkooper, R. H.; Cantó, C.; Wanders, R. J.; Auwerx, J. *Endocrine Rev.* **2010**, *31*, 194.
(b) Sauve, A. A. *J. Pharmacol. Exp. Ther.* **2008**, *324*, 883.
- (a) Galli, U.; Travelli, C.; Massarotti, A.; Fakhfour, G.; Rahimian, R.; Tron, G. C.; Genazzani, A. A. *J. Med. Chem.* **2013**, DOI: 10.1021/jm4001049. (b) He, J.; Tu, C.; Li, M.; Wang, S.; Guan, X.; Lin, J.; Li, Z. *Curr. Pharm. Des.* **2012**, *18*, 6123. (c) Burgos, E. S. *Curr. Med. Chem.* **2011**, *18*, 1947. (d) Bi, T.-q.; Che, X.-m. *Cancer Biol. Ther.* **2010**, *10*, 119. (e) Garten, A.; Petzold, S.; Körner, A.; Imai, S.-i.; Kiess, W. *Trends Endocrin. Metab.* **2008**, *20*, 130.
- In contrast, the de novo NAD synthesis pathway requires eight enzyme-catalyzed steps to produce the co-factor from tryptophan. See ref. 1 for additional details.
- (a) Schulze, A.; Harris, A. L. *Nature* **2012**, *491*, 364. (b) Chiarugi, A.; Dölle, C.; Felici, R.; Ziegler, M. *Nat. Rev. Cancer* **2012**, *12*, 741. (c) Zhang, L. Q.; Heruth, D. P.; Ye, S. Q. *J. Bioanal. Biomed.* **2011**, *3*, 13. (d) Khan, J. A.; Forouhar, F.; Tao, X.; Tong, L. *Expert Opin. Ther. Targets* **2007**, *11*, 695.
- (a) Watson, M.; Roulston, A.; Bélec, L.; Billot, X.; Marcellus, R.; Bédard, D.; Bernier, C.; Branchaud, S.; Chan, H.; Dairi, K.; Gilbert, K.; Goulet, D.; Gratton, M.-O.; Isakau, H.; Jang, A.; Khadir, A.; Koch, E.; Lavoie, M.; Lawless, M.; Nguyen, M.; Paquette, D.; Turcotte, E.; Berger, A.; Mitchell, M.; Shore, G. C.; Beauparlant, P. *Mol. Cell. Biol.* **2009**, *29*, 5872. (b) Ravaut, A.; Cerny, T.; Terret, C.; Wanders, J.; Bui, B. N.; Hess, D.; Droz, J.-P.; Fumoleau, P.; Twelves, C. *Eur. J. Cancer* **2005**, *41*, 702. (c) Hovstadius, P.; Larsson, R.; Jonsson, E.; Skov, T.; Kissmeyer, A.-M.; Krasilnikoff, K.; Bergh, J.; Karlsson, M. O.; Lönnebo, A.; Ahlgren, J. *Clin. Cancer Res.* **2002**, *8*, 2843. Compound **1** is also known in the literature as CHS828.

6. Beuparlant, P.; Bédard, D.; Bernier, C.; Chan, H.; Gilbert, K.; Goulet, D.; Gratton, M.-O.; Lavoie, M.; Roulston, A.; Turcotte, E.; Watson, M. *Anti-Cancer Drugs*, **2009**, *20*, 346.
7. (a) Olesen, U. H.; Thougard, A. V.; Jensen, P. B.; Sehested, M. *Mol. Cancer Ther.* **2010**, *9*, 1609. (b) Holen, K.; Saltz, L. B.; Hollywood, E.; Burk, K.; Hanauske, A.-R. *Invest. New Drugs* **2008**, *26*, 45. Compound **2** is also known in the literature as FK866.
8. Zheng, X.; Bauer, P.; Baumeister, T.; Buckmelter, A. J.; Caligiuri, M.; Clodfelter, K. H.; Han, B.; Ho, Y.-C.; Kley, N.; Lin, J.; Reynolds, D. J.; Sharma, G.; Smith, C. C.; Wang, Z.; Dragovich, P. S.; Gunzner-Toste, J.; Liederer, B. M.; Ly, J.; O'Brien, T.; Oh, A.; Wang, L.; Wang, W.; Xiao, Y.; Zak, M.; Zhao, G.; Yuen, P.-w.; Bair, K. W. *J. Med. Chem.* **2013**, DOI: 10.1021/jm4008664.
9. For other recently disclosed examples of NAMPT inhibitors, see: (a) Dragovich, P. S.; Bair, K. W.; Baumeister, T.; Ho, Y.-C.; Liederer, B. M.; Liu, X.; Liu, Y.; O'Brien, T.; Oeh, J.; Sampath, D.; Skelton, N.; Wang, L.; Wang, W.; Wu, H.; Xiao, Y.; Yuen, P.-w.; Zak, M.; Zhang, L.; Zheng, X. *Bioorg. Med. Chem. Lett.* **2013**, *23*, 4875. (b) Zheng, X.; Bauer, P.; Baumeister, T.; Buckmelter, A. J.; Caligiuri, M.; Clodfelter, K. H.; Han, B.; Ho, Y.-C.; Kley, N.; Lin, J.; Reynolds, D. J.; Sharma, G.; Smith, C. C.; Wang, Z.; Dragovich, P. S.; Oh, A.; Wang, W.; Zak, M.; Gunzner-Toste, J.; Zhao, G.; Yuen, P.-w.; Bair, K. W. *J. Med. Chem.* **2013**, *56*, 4921. (c) Gunzner-Toste, J.; Zhao, G.; Bauer, P.; Baumeister, T.; Buckmelter, A. J.; Caligiuri, M.; Clodfelter, K. H.; Fu, B.; Han, B.; Ho, Y.-C.; Kley, N.; Liang, X.; Liederer, B. M.; Lin, J.; Mukadam, S.; O'Brien, T.; Oh, A.; Reynolds, D. J.; Sharma, G.; Skelton, N.; Smith, C. C.; Sodhi, J.; Wang, W.; Wang, Z.; Xiao, Y.; Yuen, P.-w.; Zak, M.; Zhang, L.; Zheng, X.; Bair, K. W.; Dragovich, P. S. *Bioorg. Med. Chem. Lett.* **2013**, *23*, 3531. (d) Curtin, M. L.; Sorensen, B. K.; Heyman, H. R.; Clark, R. F.; Woller, K. R.; Shah, O. J.; Michaelides, M.; Tse, C.;

Vasudevan, A.; Mack, H.; Hansen, T. M.; Sweis, R.; Pliushchev, M. A. US 2012/0122842. (e) Kumar, D. V.; Slattum, P. M.; Yager, K. M.; Shenderovich, M. D.; Tangallapally, R.; Kim, S.-H. WO 2012/177782. (f) You, H.; Youn, H.-S.; Im, I.; Bae, M.-H.; Lee, S.-K.; Ko, H.; Eom, S. H.; Kim, Y.-C. *Eur. J. Med. Chem.* **2011**, *46*, 1153.

10. (a) Chiang, P.-W.; Wang, J.; Chen, Y.; Fu, Q.; Zhong, J.; Chen, Y.; Yi, X.; Wu, R.; Gan, H.; Shi, Y.; Chen, Y.; Barnett, C.; Wheaton, D.; Day, M.; Sutherland, J.; Heon, E.; Weleber, R. G.; Gabriel, L. A. R.; Cong, P.; Chuang, K.; Ye, S.; Sallum, J. M. F.; Qi, M. *Nat. Genet.* **2012**, *44*, 972. (b) Perrault, I.; Hanein, S.; Zanlonghi, X.; Serre, V.; Nicouleau, M.; Defoort-Delhemmes, S.; Delphin, N.; Fares-Taie, L.; Gerber, S.; Xerri, O.; Edelson, C.; Goldenberg, A.; Alice Duncombe, A.; Le Meur, G.; Hamel, C.; Silva, E.; Nitschke, P.; Calvas, P.; Munnich, A.; Roche, O.; Dollfus, H.; Kaplan J.; Rozet, J.-M. *Nat. Genet.* **2012**, *44*, 975. (c) Koenekoop, R. K.; Wang, H.; Majewski, J.; Wang, X.; Lopez, I.; Ren, H.; Chen, Y.; Li, Y.; Fishman, G. A.; Genead, M.; Schwartzenruber, J.; Solanki, N.; Traboulsi, E. I.; Cheng, J.; Logan, C. V.; McKibbin, M.; Hayward, B. E.; Parry, D. A.; Johnson, C. A.; Nageeb, M.; Poulter, J. A.; Mohamed, M. D.; Jafri, H.; Rashid, Y.; Taylor, G. R.; Keser, V.; Mardon, G.; Xu, H.; Inglehearn, C. F.; Fu, Q.; Toomes C.; Chen, R. *Nat. Genet.* **2012**, *44*, 1035. (d) Falk, M. J.; Zhang, Q.; Nakamaru-Ogiso, E.; Kannabiran, C.; Fonseca-Kelly, Z.; Chakarova, C.; Audou, I.; Mackay, D. S.; Zeitz, C.; Borman, A. D.; Staniszevska, M.; Shukla, R.; Palavalli, L.; Mohand-Said, S.; Waseem, N. H.; Jalali, S.; Perin, J. C.; Place, E.; Ostrovsky, J.; Xiao, R.; Bhattacharya, S. S.; Consugar, M.; Webster, A. R.; Sahel, J.-A.; Moore, A. T.; Berson, E. L.; Liu, Q.; Gai, X.; Pierce E. A. *Nat. Genet.* **2012**, *44*, 1040.

11. Humans who are heterozygous carriers of the described NMNAT mutations do not exhibit the LCA phenotype. In addition, the enzymatic activity of the mutant NMNAT proteins is only

partially impaired relative to wild type enzyme, and NAD levels measured in RBCs from a homozygous mutation carrier were approximately 70% of those observed in RBCs from a heterozygous comparator (see ref. 10a-d for additional details).

12. Ophthalmologic evaluations (ERG and visual acuity) were a component of patient monitoring performed during the clinical trials of compound **2**. No concerns regarding the retinal health of participating patients were noted. See ref. 7b for additional details.

13. HSP90 inhibitors which exhibit reduced retinal penetration and/or retention cause minimal (none) retinal damage in rodents relative to molecules with higher retinal exposures. See: Zhou, D.; Teofilovici, F.; Liu, Y.; Ye, J.; Ying, W.; Ogawa, L. S.; Inoue, T.; Lee, W.; Adjiri-Awere, A.; Kolodzieyski, L.; Tatsuta, N.; Wada, Y.; Sonderfan, A. J. American Society of Clinical Oncology Annual Meeting, Chicago, IL, June 1-5, **2012**; Abstract #3086.

14. (a) Hosoya, K.-i.; Tomi, M.; Tachikawa, M. *Expert Opin. Drug Deliv.* **2011**, *8*, 1571. (b) Toda, R.; Kawazu, K.; Oyabu, M.; Miyazaki, T.; Kiuchi, Y. *J. Pharm. Sci.* **2011**, *100*, 3904. (c) Kadam, R. S.; Kompella, U. B. *J. Pharmacol. Exp. Ther.* **2010**, *332*, 1107.

15. We currently believe that many potent NAMPT inhibitors form PRPP-derived phosphoribosylated adducts in the protein's active site which block the function of the enzyme. This belief is consistent with the repeated observation of these adducts by mass spectrometry in biochemical experiments (see refs. 5a, and 8) and with crystallographic observation of these entities in complex with NAMPT (ref. 22 and this work). Once formed, the PRPP-adducts may accumulate intracellularly and thereby enhance cell culture antiproliferation effects (see ref. 5a for additional information and discussion). However, there are many other factors that also likely influence NAMPT inhibitor cell potency including: biochemical potency, the ability of a given inhibitor and/or its corresponding PRPP-derived ribose adduct to effectively compete with

the NAM substrate, cell membrane permeability, and/or protein binding. In addition, performing the PRPP-adduct assessments was a relatively resource-intensive task and such determinations were therefore made for only a small number of compounds.

16. The antiproliferative effects exhibited in cell culture by **13** were completely eliminated ("reversed") when the compound was tested in the presence of 0.33 mM NMN (the product of the NAMPT-catalyzed condensation of nicotinamide and PRPP; c.f., Figure 1). This result strongly suggests that the observed cell-based effects result from NAMPT inhibition. Related NMN experiments were conducted in cell-based assessments with all inhibitors reported in this work and all displayed similar reversals of their antiproliferative effects.

17. All compounds which contain the bicyclic heterocycle present in inhibitor **13** are referred to as *1H*-pyrazolo[3,4-*b*]pyridines throughout this work.

18. NAMPT is believed to function as a symmetrical homodimer with two active sites formed at opposite ends of the dimer interface. Accordingly, the protein crystalized with such a dimer present in the asymmetric unit. The two monomer chains were highly similar (RMSD 0.13 Å for 413 C-alpha atoms, as defined by the protein alignment tool in PyMOL) and both active sites contained a molecule of compound **14** in a similar orientation. In the crystallography discussion, the NAMPT residues are designated with prime and non-prime notation (e.g., Tyr18', Phe193) to distinguish the monomer chain in which a given residue resides. PDB code = 4M6P.

19. A caveat with comparing the retinal exposures of compounds **4** and **26** is that the described results were obtained from experiments that employed different dosing regimens. Compound **4** was dosed for two consecutive days and was co-administered with nicotinic acid while compound **26** was administered once as a single-agent. However, based on the measured disappearance of **4** from rat retina over time (Table 5), we do not believe that significant

accumulation of the compound occurred during the 2-day experiment relative to what would be observed following a single dose. We also do not believe that nicotinic acid co-administration impacted the retinal exposures of **4**, although we did not generate data to explore this hypothesis.

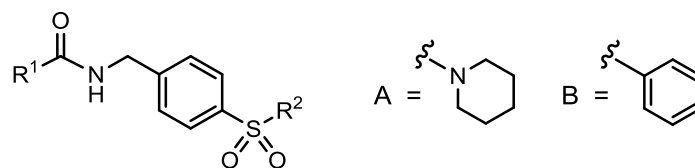
20. Day-5 exposures of **4** and **26** are depicted in Figure S5A. The day-1 exposure of each compound was very similar to the corresponding day-5 exposure (data not shown). Compound exposures on other study days were not assessed.

21. The mouse plasma protein binding properties of inhibitors **4** and **26** differ by <6-fold ($f_u = 0.067$ and 0.013 , respectively) and thus do not easily explain the NAD PK-PD study outcomes.

22. PDB code = 4M6Q. The two NAMPT monomer chains which formed the symmetrical protein homodimer were highly similar (RMSD 0.17 \AA for 426 C-alpha atoms as defined by the protein alignment tool in PyMOL) and both active sites contained a molecule of the **26**-PRPP adduct in a similar orientation

23. Wang, W. manuscript in preparation.

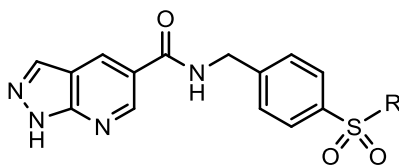
24. Burgos, E. S.; Vetticatt, M. J.; Schramm, V. L. *J. Am. Chem. Soc.* **2013**, *135*, 3485.

Table 1. Initial structure-activity relationships.

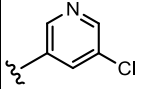
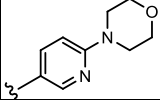
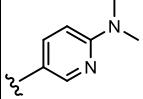
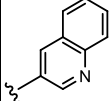
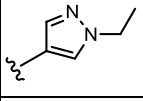
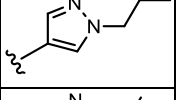
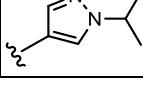
Cmpd.	R ¹	R ²	NAMPT IC ₅₀ (μ M) ^a	A2780 IC ₅₀ (μ M) ^b
3		A	0.028	0.006
9		B	0.018	0.013
10		A	>2.0	>2.0
11		B	1.3	>2.0
12		B	>2.0	>2.0
13		A	0.10	0.088
14		B	0.054	0.066
15		B	1.7	>2.0
16		B	1.9	>2.0

See supplementary data for experimental details associated with each assessment. All biochemical and cell-based assay results are reported as the arithmetic mean of at least 2 separate runs.

^aNAMPT biochemical inhibition. ^bAntiproliferation activity determined in cell culture experiments using A2780 cell line. This inhibition can be reversed by addition of 0.33 mM of NMN.

Table 2. Structure-activity relationships of 1*H*-pyrazolo[3,4-*b*]pyridine-containing NAMPT inhibitors.

Cmpd.	R	NAMPT IC ₅₀ (uM) ^a	A2780 IC ₅₀ (uM) ^b	HLM CL _{hep} (mL/min/kg) ^c
13		0.10	0.088	18
17		0.41	>2.0	16
18		0.40	0.039	17
19		0.41	0.21	11
20		0.39	0.33	5.4
21		0.30	0.035	8.6
22		0.44	0.045	7.6
23		0.37	0.28	6.7
24		0.11	0.045	11
14		0.054	0.066	4.4
25		0.0079	0.0060	9.1
26		0.0061	0.0043	8.8
27		0.0077	0.0048	7.6
28		0.010	0.0045	7.2

29		0.011	0.0024	13
30		0.0045	0.0013	11
31		0.012	0.0032	14
32		0.0082	0.0022	13
33		0.19	0.031	6.0
34		0.010	0.0069	6.3
35		0.099	0.012	4.4

See supplementary data for experimental details associated with each assessment. All biochemical, cell-based assay, and HLM results are reported as the arithmetic mean of at least 2 separate runs.

^aNAMPT biochemical inhibition. ^bAntiproliferation activity determined in cell culture experiments using A2780 cell line. This inhibition can be reversed by addition of 0.33 mM of NMN. ^cHuman hepatic clearance predicted from human liver microsomes (stable, moderate, labile = <6, 6-15, >15 mL/min/kg, respectively).

Table 3. *In vitro* DMPK properties of selected NAMPT inhibitors.

Cmpd.	MLM CL _{hep} (mL/min/kg) ^a	MH CL _{hep} (mL/min/kg) ^b	MDCK P _{app,A-B} ; x10 ⁻⁶ cm/s ^c	Mouse PPB (f _u) ^d	Sol. (uM) ^e
25	69	22	7.8	0.114	<1.0
26	42	13	11	0.013	1.4
27	42	8	4.0	0.008	<1.0
28	65	18	4.4	0.050	<1.0
29	76	24	2.5	0.074	<1.0
30	65	31	0.85	0.019	<1.0
31	77	45	1.5	0.018	<1.0
32	73	44	1.6	0.009	<1.0
34	63	27	1.9	0.071	8.8

See supplementary data for experimental details associated with each assessment. All assay results are reported as the arithmetic mean of at least 2 separate runs (exception: solubility determinations are n = 1).

^aMouse hepatic clearance predicted from mouse liver microsomes (stable, moderate, labile = <27, 27-63, >63 mL/min/kg, respectively). ^bMouse hepatic clearance predicted from mouse hepatocytes (stable, moderate, labile = <27, 27-63, >63 mL/min/kg, respectively). Apparent permeability coefficients (P_{app,A-B}) across MDCK cell monolayers ^dMouse plasma protein binding; fraction unbound (f_u). ^eAqueous solubility.

Table 4. *In vivo* DMPK properties of compound **26** in female nude mice.

Route	Dose (mg/kg) ^a	C _{max} (μM) ^b	T _{max} (h) ^c	V _{ss} (L/kg) ^d	CL (mL/min/kg) ^e	T _{1/2} (h) ^f
IV	5	NA	NA	0.45	3.3	2.6
PO	100	53	0.25	NA	NA	3.4

^aFormulations: IV = 35:10:15:40 PEG400:EtOH:PG:Water (solution); PO = 60:10:30 PEG400:EtOH:Water (solution). ^bMaximum plasma concentration. ^cTime at which maximum plasma concentration observed. ^dVolume of distribution (steady-state). ^eClearance. ^fHalf-life. NA = not applicable. See supplementary data for experimental descriptions.

Table 5. Retina concentration and retina/plasma ratio (both uncorrected for protein binding effects) determined in rats for compounds **4** and **26** at indicated timepoints following a 30 mg/kg oral dose of each molecule (n = 4 for **4**; n = 3 for **26**). Standard deviations are also provided. See supplementary data for additional information.

Cmpd.	[Retina] (μM)		Retina/Plasma Ratio	
	1 h	6.5 h	1 h	6.5 h
4^a	1.9 \pm 0.82	1.3 \pm 0.31	0.32 \pm 0.11	0.30 \pm 0.12
26	0.94 \pm 0.23	0.68 \pm 0.23	0.071 \pm 0.006	0.093 \pm 0.036

^aCompound was dosed QD for 2 consecutive days in combination with 75 mg/kg nicotinic acid that was administered orally BID. Data were obtained following day 2 dose.

Table 6. Biochemical inhibition activity (IC₅₀ in nM) of compounds **4** and **26** as determined against NAMPT enzymes from indicated species.^{a,b}

Cmpd.	NAMPT Biochemical IC ₅₀ Values (nM)				
	Human	Mouse	Rat	Dog	Monkey
4	5	24	23	7	42
26	6	59	35	22	73

^aReported as the arithmetic mean of at least 2 separate runs. ^bPRPP-ribose adduct formation detected for both compounds in every species. See supplementary data for additional information.

Table 7. Antiproliferation effects of compounds **4** and **26** determined in various cell lines from different animal species.^a

Species	Cell Line	CyQuant IC ₅₀ values in nM	
		Cmpd. 4	Cmpd. 26
Human	HT1080	2	9
	PC3	3	9
	MiaPaCa2	7	30
	HCT116	2	8
	Calu6	5	21
Mouse	KPP	16	775
	KPR	41	>1000
	B16F10	71	>1000
Dog	A-72	4	23
	D-17	12	98
	DH-82	7	41
Monkey	Cos1	5	501
	Cos7	9	863
	RF/6A	4	386

^aReported as the arithmetic mean of 3 separate runs. See supplementary data for additional information.

Table 8. Ability of compounds **4** and **26** to reduce NAD levels in human and mouse cell lines.

Cmpd.	PC3 (human)			KPP (mouse)		
	EC ₅₀ (nM) ^a	[Cell-1] ^b	[Cell-2] ^c	EC ₅₀ (nM) ^a	[Cell-1] ^b	[Cell-2] ^c
4	1.1	9	30	1.3	8	31
26	1.2	10	54	70	12	74

Data are reported as average of two independent experiments which utilized triplicate samples in each run. See supplementary data for additional information.

^aNAD inhibition activity in given cell line. ^bIntracellular concentration (nM) of **4** and **26** measured during NAD inhibition experiment in given cell line; extracellular concentration in well = 200 nM. ^cIntracellular concentration (nM) of **4** and **26** measured during NAD inhibition experiment in given cell line; extracellular concentration in well = 1000 nM.

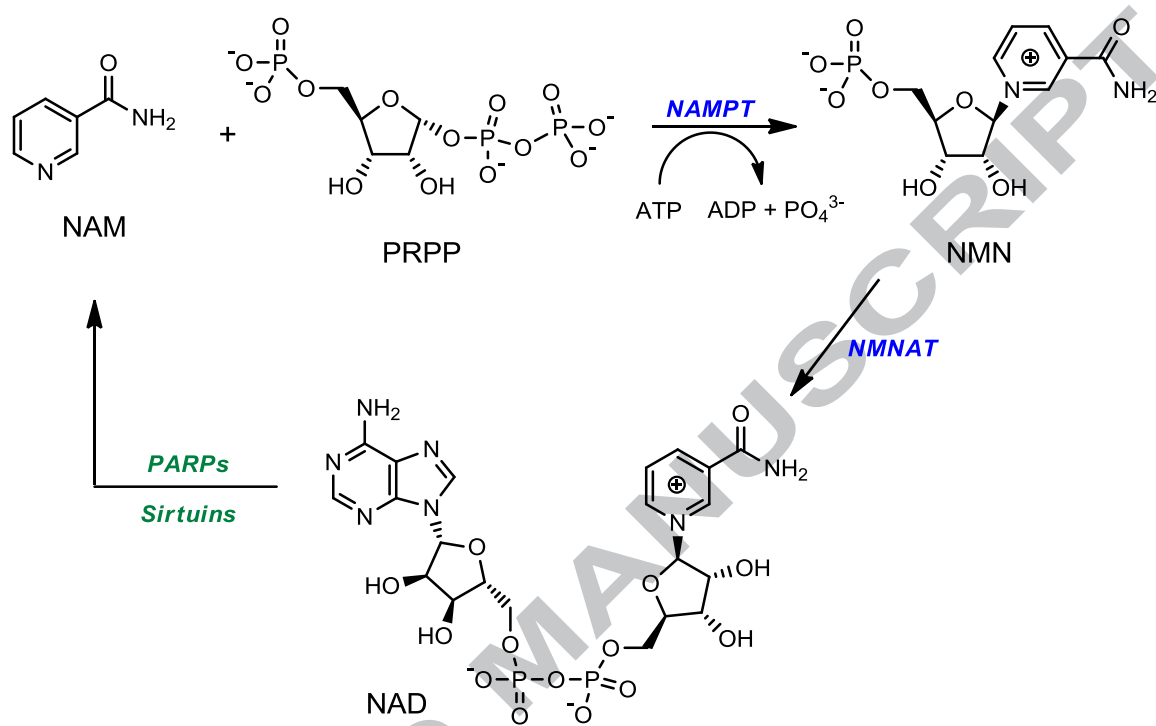
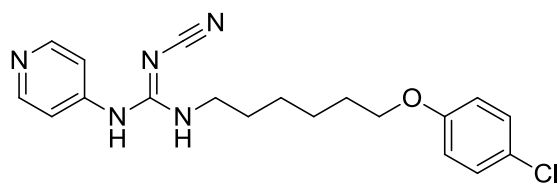
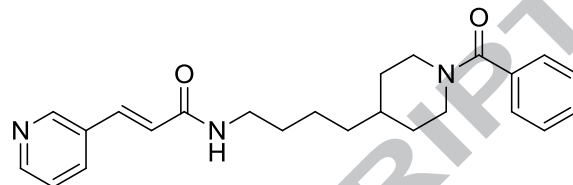
Figure 1. NAD recycling and NAMPT biochemical mechanism.

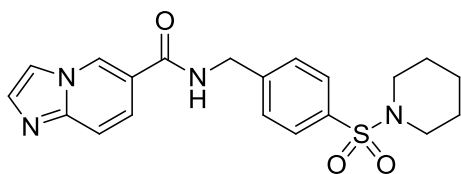
Figure 2. Examples of NAMPT inhibitors.



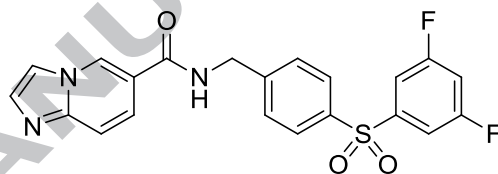
1 (GMX-1778)



2 (APO-866)



3



4

Figure 3. Design of 1*H*-pyrazolo[3,4-*b*]pyridine as NAMPT inhibitors.

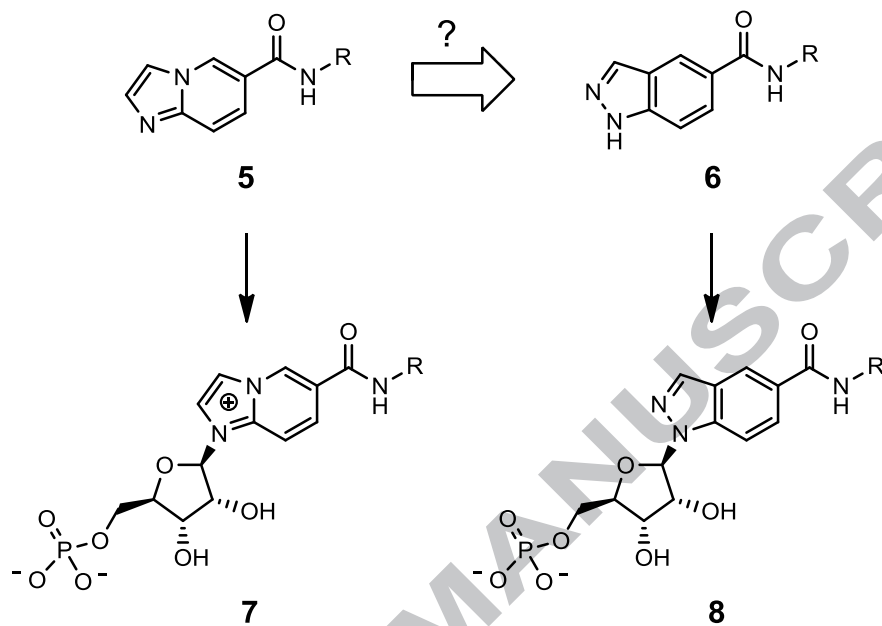


Figure 4. Co-crystal structure of inhibitor **14** (green) in complex with human NAMPT (PDB code = 4M6P). The ligand binds to a site formed by the interface of two NAMPT protein monomers (depicted as white and cyan, respectively). Water molecules are depicted as red spheres. Hydrogen bonds are indicated with dashed yellow lines, and the van der Waals surface of the protein is shown in grey. A phosphate molecule (orange), likely originating from the crystallization buffer, is also depicted. The resolution of the structure is 1.75 Å. The figure was generated using the program PyMOL, from Schrödinger, LLC (version 1.5.0.4).

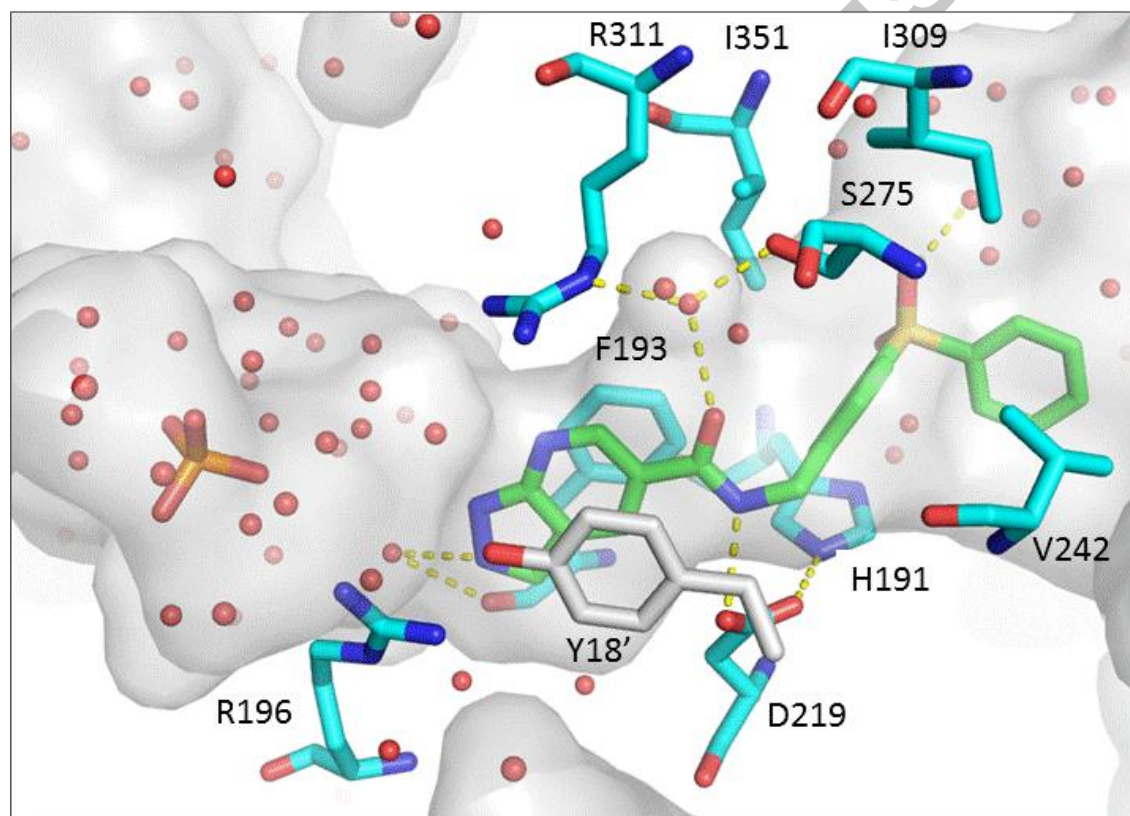


Figure 5. Mean (\pm standard deviation) plasma concentration-time profiles of compound **26** in female nude mice following intravenous and oral administration.

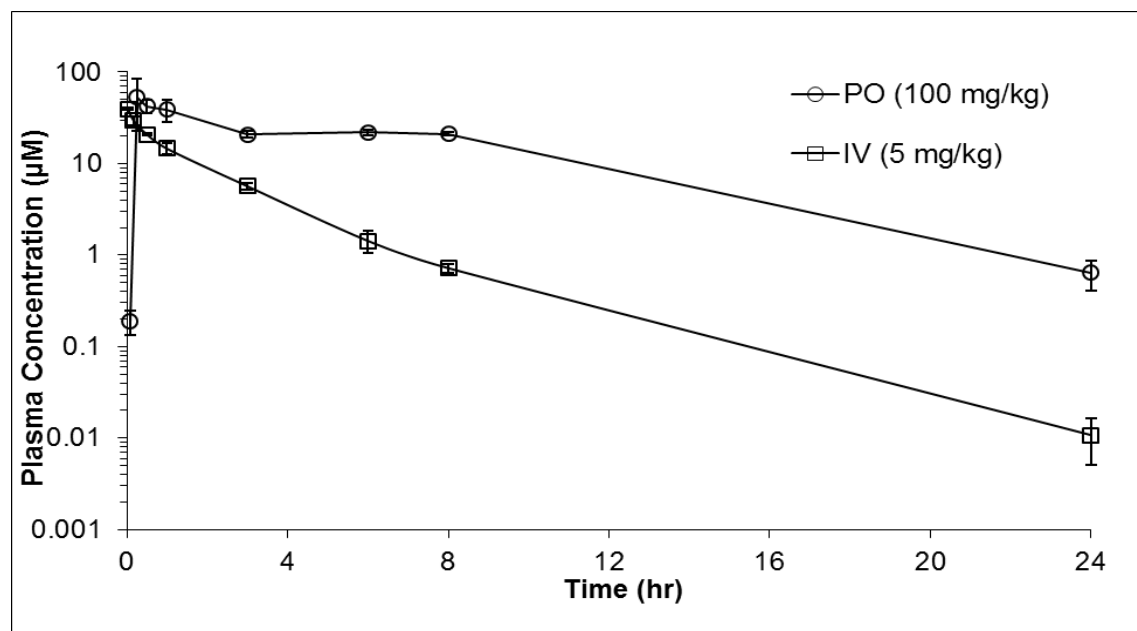
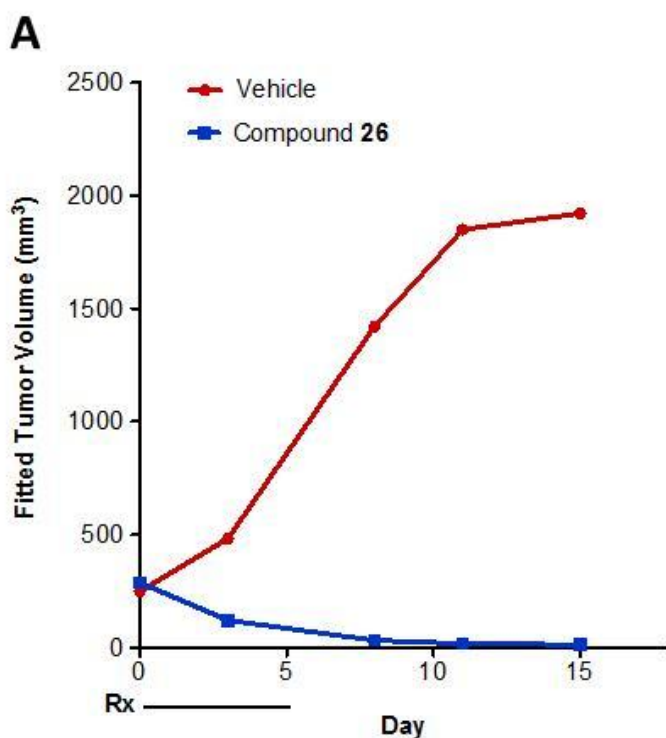


Figure 6. Efficacy and pharmacodynamics of compound **26** dosed orally QD for 5 days at 100 mg/kg in the A2780 human ovarian cancer xenograft model. Vehicle = 60% PEG400 / 10% EtOH / 30% D5W. **A.** Xenograft efficacy. Data reflect fitted tumor volumes (mm^3). Rx = treatment period. **B.** Tumor NAD levels and plasma concentrations of compound **26** measured at indicated time-point following day-5 dose. Error bars indicate \pm standard deviations. See supplementary data for additional details.



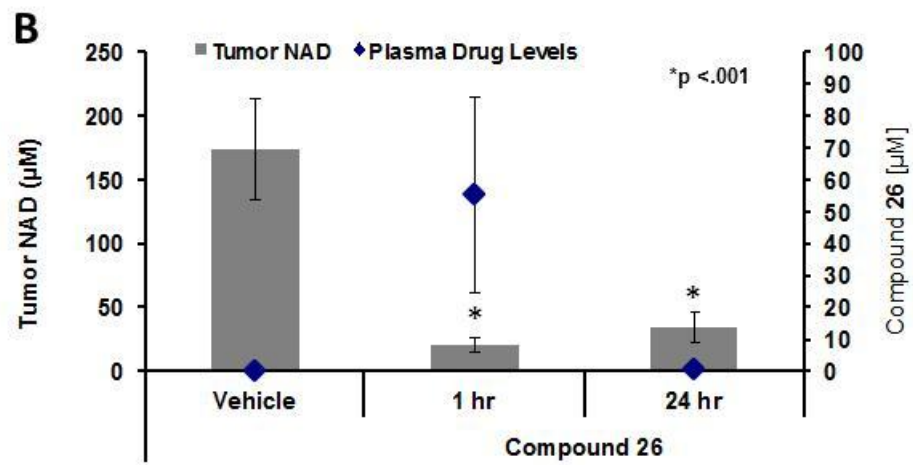


Figure 7. Co-crystal structure of the PRPP- ribosylated adduct corresponding to compound **26** (purple) in complex with human NAMPT (PDB code = 4M6Q). The ligand binds to a site formed by the interface of two NAMPT protein monomers (depicted as white and cyan, respectively). Water molecules are depicted as red spheres. Hydrogen bonds are indicated with dashed yellow lines, and the van der Waals surface of the protein is shown in grey. A pyrophosphate moiety is also depicted in orange, and the red dotted line indicates the distance between one of its terminal oxygen atoms and the C1' ribose atom of the **26**-ribose adduct (3.5 Å). The resolution of the structure is 2.40 Å. The previously determined bound conformation of inhibitor **14** (green) is superimposed for comparison. The figure was generated using the program PyMOL, from Schrödinger, LLC (version 1.5.0.4).

